Journal of Magnetism and Magnetic Materials 322 (2010) 3834–3840

Contents lists available at ScienceDirect

Journal of Magnetism and Magnetic Materials

journal homepage: www.elsevier.com/locate/jmmm

Size analysis and magnetic structure of nickel nanoparticles

D.-X. Chen [a,*], O. Pascu [b], A. Roig [b], A. Sanchez [c]

[a] ICREA and Departament de Física, Universitat Autònoma de Barcelona, 08193 Bellaterra, Spain
[b] Institut de Ciència de Materials de Barcelona (ICMAB), CSIC, 08193 Bellaterra, Spain
[c] Departament de Física, Universitat Autònoma de Barcelona, 08193 Bellaterra, Spain

ARTICLE INFO

Article history:
Received 22 May 2010
Received in revised form
31 July 2010
Available online 7 August 2010

Keywords:
Magnetization curve
Metallic ferromagnetic nanoparticle
Particle size determination
Core–shell model

ABSTRACT

The size distribution of an assembly of fcc nickel nanoparticles is studied by measuring the temperature dependent magnetization curves fitted by a uniform model and a core–shell model, both based on the Langevin function for superparamagnetism with a log-normal particle volume distribution. The uniform model fits lead to a spontaneous magnetization M_s much smaller than the M_s for bulk nickel and to particle sizes larger than the ones evaluated by transmission electron microscopy; the core–shell model fits can result in a correct size distribution but the M_s in the core becomes significantly greater than the M_s for bulk nickel. It is concluded that there is a core–shell magnetic structure in nickel particles. Although the enhanced M_s in the core may be related to the narrowing of the energy bands of 3d electrons in small fcc nickel particles, the modeling values of M_s are over large compared with previous calculations on nickel clusters of different structures, which implies possible existence of an exchange interaction between the core and the shell, which is not considered in the simple core–shell model.

1. Introduction

Ferrimagnetic or ferromagnetic fine particles present rich physical phenomena and also serve as a key element in many technologies, including recent developments in fields such as magnetic separation, drug delivery, hyperthermia treatments and magnetic resonance imaging contrast agents [1], which have followed earlier applications in magnetic recording and ferromagnetic liquids [2,3]. In most cases, a knowledge of size distribution of the fine particles is crucially important for the proper working of a particular application.

The magnetic particle size distribution of powder samples may be determined from the measurements of magnetization curve based on the theory of superparamagnetism, first proposed by Bean and co-workers [4–6]. This theory defines a dilute assembly of ferromagnetic particles as superparamagnetic if the particles are single domain and when the thermal energy at the temperature of the experiment is sufficient to equilibrate the magnetization of the assembly in a time shorter than that of the experiment. The reduced magnetization $M(H)$ curve of the superparamagnetic assembly is expressed by the Langevin function

$$L(x) = \coth x - 1/x, \tag{1}$$

where $x = \mu_0 m_0 H/k_B T$, with m_0, k_B, and T being the particle magnetic moment, the Boltzmann constant, and temperature, respectively [6]. Thus, the particle moment may be determined by magnetic measurements, from which the particle volume may be obtained as m_0/M_s if the saturation magnetization M_s is known.

The saturation magnetization of particles M_s was first thought to be the same as for the bulk material that had the same composition and structure as the particles. However, already in 1968, M_s of many acicular γ–Fe_2O_3 polycrystalline particles was measured at room temperature, and it was found that M_s decreased with decreasing the average crystallite size determined from X-ray diffraction (XRD) line broadening measurements using the Scherrer relation [7]. This phenomenon was explained by assuming the crystallites to be separated by a nonmagnetic grain shell on the order of 0.6 nm thick. A similar effect was found for single-domain superparamagnetic Fe_3O_4 particles in ferromagnetic liquids; their magnetization curve could be correlated to the superparamagnetic theory only when the size distribution of the suspended particles was considered with their volumetric concentration corrected for the formation of a nonmagnetic surface mantle one-unit-cell thick [8]. Such surface mantle was later called the magnetically dead layer with respect to the magnetic core [9]. The differences in magnetic structure between the surface layer and the core have been an interesting topic in physics [10–13].

A frequently adopted approach since then has been to assume the particles with a certain size distribution to have the same M_s as the bulk and to determine by magnetic measurements a "magnetic size", which is significantly smaller than the physical size obtained from transmission electron microscopy (TEM) data. In recent years, however, in the determination of particle sizes by magnetic measurements, a paramagnetic susceptibility term has

* Corresponding author.
E-mail address: duxing.chen@uab.es (D.-X. Chen).

0304-8853/$ - see front matter © 2010 Elsevier B.V. All rights reserved.
doi:10.1016/j.jmmm.2010.07.046

been incorporated to the superparamagnetic term, and the magnetically determined sizes of Fe_3O_4 or $\gamma-Fe_2O_3$ nanoparticles are found to be in agreement with the sizes determined by TEM or XRD techniques [14–16]. In [17], we have completed this approach by proposing a core–shell model and a uniform model, both based on the Langevin function with a log-normal particle volume distribution, and by performing careful fits to experimental data of iron-oxide nanoparticles. It has been found that the core–shell model gives particle sizes consistent with the TEM or XRD sizes, while the sizes determined by the uniform model are larger with a wider distribution. The core–shell model has been used for the size analysis of superparamagnetic iron-oxide particles, which could be used potentially as contrast agents of magnetic resonance imaging [18].

In this work, we will use the methodology developed in [17] to study ferromagnetic nickel nanoparticles, to be compared with experimental and theoretical results on similar particles already published in the literature [19–29]. We will show that our particles display interesting magnetic features different from ferrimagnetic iron-oxide nanoparticles.

2. Experimental

2.1. Synthesis of nickel nanoparticles

Nickel nanoparticles were synthesized by thermal decomposition of a nickel organometallic precursor, adapting the method reported in [27]. For the studied particles, 1 mmol of $Ni(acac)_2$ was added to 7 ml oleylamine and 3 mmol trioctylphosphine, and the mixture was heated to 130 °C and stirred magnetically under a flow of high purity argon gas for 20 min, and then further heated to 250 °C and maintained at this temperature for 30 min. After cooling to room temperature, the nanoparticles were precipitated by adding excessive ethanol, followed by centrifugation. The as-prepared precipitate was dried at 70 °C overnight then weighted. To prevent oxidation, the as-synthesized nickel nanoparticles were kept as a concentrated dispersion in hexane of a known concentration.

2.2. Characterization of nanoparticles

TEM and XRD were used for morphological and structural characterization of the nanoparticles. TEM images were obtained using a JEOL JEM-2011 electron microscope, operating at 200 kV. The sample was prepared by depositing a drop of dilute nanoparticles hexane dispersion onto a TEM carbon grid followed by room temperature drying. A representative TEM image is shown in Fig. 1, where we see that most particles are roughly spherical.

XRD was performed for a powder sample by a Rigaku diffractometer with Cu Kα incident radiation ($\lambda = 0.154$ nm). The resulting pattern is shown in Fig. 2, from which four peaks are observed corresponding to the (1 1 1), (2 0 0), (2 2 0), and (3 1 1) planes of fcc structure of lattice parameter 0.354 nm (very near the standard value 0.352 nm for bulk nickel). The average crystallite size may be determined from XRD pattern using the Scherrer relation with a shape factor of 4/3 for spherical particles [30]

$$D_{\mathrm{XRD}} = \frac{4k\lambda}{3\Delta(2\theta)\cos\theta}, \tag{2}$$

where Scherrer constant $k=0.9$, the peak is centered at 2θ, and $\Delta(2\theta)$ (rad) is the width of the peak at half maximum intensity. The D_{XRD} determined from the (1 1 1), (2 0 0), (2 2 0), and (3 1 1) peaks is 5.2, 3.4, 5.2, and 4.5 nm, respectively.

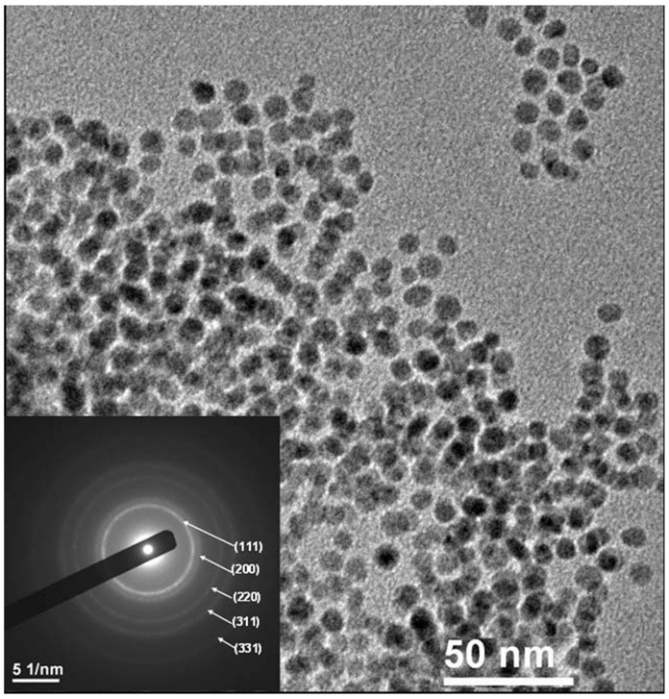

Fig. 1. TEM image of studied nanoparticles. The inset is a selected area electron diffraction pattern with indexed planes.

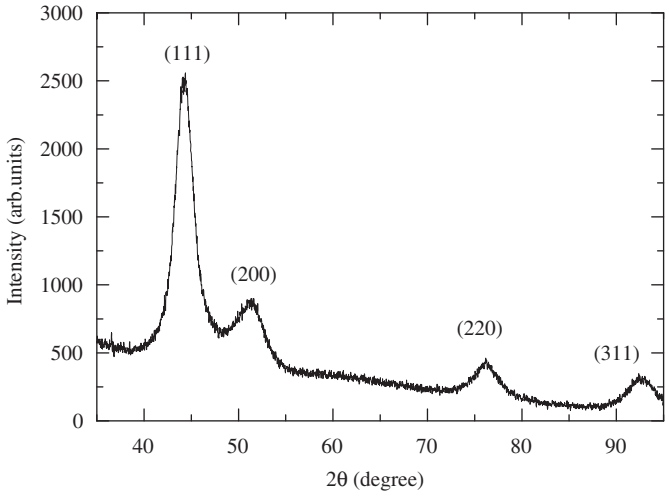

Fig. 2. The X-ray diffraction pattern of studied nanoparticles.

2.3. Magnetic measurements

The magnetic measurements were performed with a superconducting quantum interference device (SQUID) magnetometer, which was carefully calibrated by using a Pd standard sample. The nickel sample was powder packed in a plastic capsule. The zero-field and field (3 kA/m) cooled measurements were carried out for one sample during warming at a measuring applied field $H_a = 3$ kA/m. The results are shown in Fig. 3, from which we see that the external susceptibility M/H_a increases and then decreases with increasing temperature T for the zero-field cooled case, whereas it decreases monotonically with T for the field cooled case and that both curves merge at $T > 75$ K.

Another sample was prepared with more caution concerning the powder mass (to get more accurate magnetization) and its

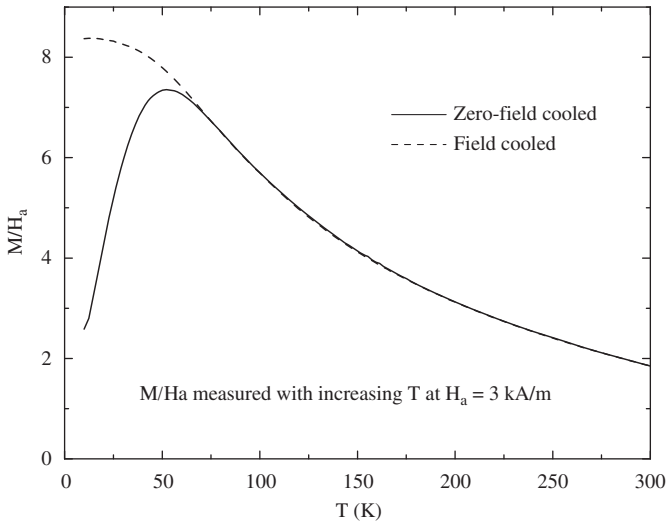

Fig. 3. External susceptibility M/H_a of a powder sample measured at H_a=3 kA/m as a function of increasing temperature T, after cooling at H_a=0 and 3 kA/m.

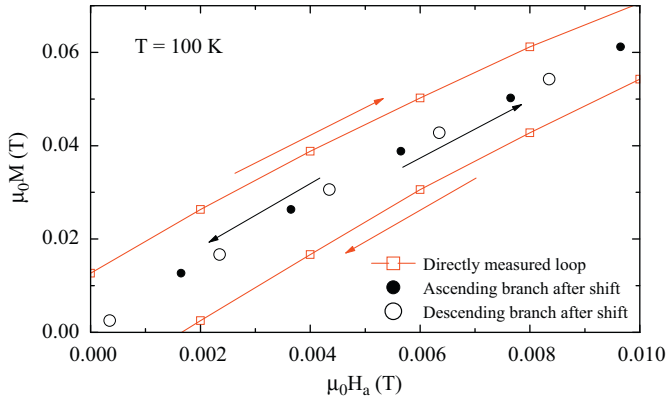

Fig. 4. The correction to $M(H_a)$ loop obtained from SQUID magnetometric measurements, showing how the unphysical measured loop (low-field portion) is shifted to a reversible magnetization curve.

dispersion (to reduce demagnetizing effects) and used for the measurements of magnetization loops at T=100, 200, 300, and 400 K. In the data treatment, a shift of $\pm$0.00165 T was performed for the ascending and descending applied field $\mu_0 H_a$ to correct the effects of remanence of the SQUID superconducting magnet, so that the magnetic reversibility of the measured sample could be accurately checked.

A comparison between the directly recorded and corrected hysteresis loops in a low-field region is shown in Fig. 4. Owing to the irreversible magnetization of the superconducting wire of which the magnet of the SQUID magnetometer is wound, the field at the magnet center is produced not only by the current flowing through the wire, from which the field reading is calculated, but also by the poles in the magnetized wire itself, which gives an error in the field measurements. According to the critical-state model [31], the magnetization of the wire will be along the field produced by the transport current when the current decreases from a large value as in our case. Thus, the poles will produce a negative demagnetizing field at the magnet center when the total field sweeps from a large positive value in the descending branch. As a result, by cycling the field between $\pm$5 T, the directly measured $M(H_a)$ of a paramagnetic sample will become a hysteresis loop corresponding unphysically to a negative energy loss, as shown in Fig. 4. Such a loop is corrected to a reversible one after a shift determined by the calibration of the SQUID magnetometer with a paramagnetic Pd standard sample. This correction is essential at low $|H_a|$ only.

Moreover, a demagnetizing correction was performed to convert the applied field H_a to the internal field H in the sample by using

$$H = H_a - N_m M, \tag{3}$$

where magnetometric demagnetizing factor N_m=0.02 was taken (see below) [32]. After such corrections, the $\mu_0 M$ vs $\mu_0 H$ loops are plotted in Fig. 5 by solid (ascending branch) and open circles (descending branch).

For calculating magnetization, the mass fraction $(1-f_m)$ of surfactants on the surface of dried nanoparticles was obtained by thermogravimetric analysis (TGA). A powder sample of about 10-mg mass was measured with a Mettler Toledo TGA/SDTA 851 at heating rate 10 °C/min in a temperature range 30–800 °C under flowing N_2.

The original data given by the magnetometer were the moment m of the sample in emu units. The formula to calculate $\mu_0 M$ in SI units is $\mu_0 M = 4\pi m\rho/(10\,000 w f_m)$, where f_m=0.83 is obtained from TGA data and w and ρ are the sample mass and the density of nickel (8.9 g/cm^3), respectively, in cgs units.

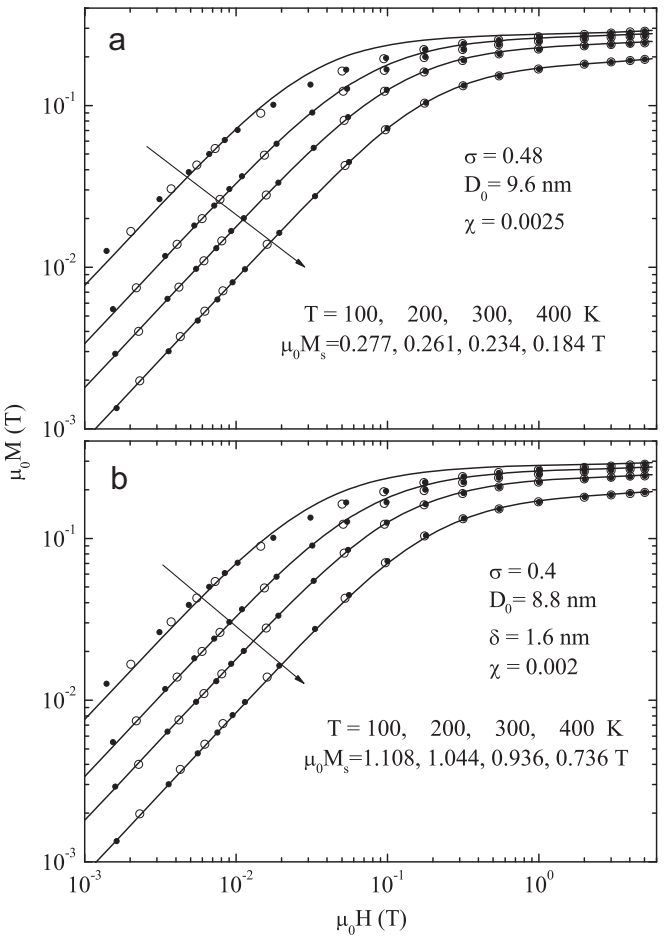

Fig. 5. The magnetization M versus field H loops (solid and open circles for ascending and descending branches, respectively) of a powder sample measured at T=100, 200, 300, and 400 K and their fits (lines) by the uniform model (a) and the core–shell model (b). Arrows indicate the direction of increasing T.

3. Model fits to magnetization curves

3.1. Uniform and core–shell models

To fit the $\mu_0 M$ versus $\mu_0 H$ curves, we assume that all particles are spherical without mutual interaction and the particle volume v distribution by volume follows the log-normal probability density function

$$p(v;\mu,\sigma)=\frac{1}{\sqrt{2\pi}\sigma v}\exp\left[-\frac{(\ln v-\mu)^2}{2\sigma^2}\right], \tag{4}$$

where μ and σ are the mean and the standard deviation of $\ln v$. For convenience, we define

$$\mu\equiv \ln v_0=\ln(\pi D_0^3/6), \tag{5}$$

where v_0 and D_0 are the median volume and its corresponding diameter, respectively.

The uniform model assumes all the particles to have the same spontaneous magnetization M_s (equal to the average saturation magnetization of the superparamagnetism for the entire particle assembly) and the same paramagnetic susceptibility χ. Magnetization M as a function of field H is contributed by the superparamagnetism and paramagnetism of all the particles with a volume distribution $p(v;\mu,\sigma)$ and is expressed by

$$M(H)=\int_0^\infty p(v;\mu,\sigma)[M_s \mathrm{L}(x)+\chi H]\,dv, \tag{6}$$

where $\mathrm{L}(x)$ is expressed by Eq. (1) with

$$x=\mu_0 M_s v H/k_B T. \tag{7}$$

The core–shell model assumes that each particle has an inner single-domain core with spontaneous magnetization M_s and an outer paramagnetic shell of susceptibility χ and thickness δ, if the particle diameter $D>2\delta$. Writing the volumes of a particle, its core, and its shell as v, v_c, and v_s, respectively, we have in general $v=v_c+v_s=\pi D^3/6$ and $v_c=0$ if $D<2\delta$ and $v_c=\pi(D-2\delta)^3/6$ otherwise. Thus, $M(H)$ is contributed by the core superparamagnetism and the shell paramagnetism of all the particles with a volume distribution $p(v;\mu,\sigma)$ and is expressed by

$$M(H)=\int_0^\infty p(v;\mu,\sigma)v^{-1}[M_s v_c \mathrm{L}(x)+v_s\chi H]\,dv, \tag{8}$$

where $\mathrm{L}(x)$ is expressed by Eq. (1) with

$$x=\mu_0 M_s v_c H/k_B T. \tag{9}$$

These uniform and core–shell models have been explained in greater detail in [17]. Most researchers used the Langevin function to fit superparamagnetic magnetization curves of particle systems without considering a paramagnetic contribution (i.e., $\chi=0$) and a magnetic core–shell structure. Although such model fits cannot be good according to our experience, we will call the model used in, for example, [24,26] without explicitly mentioning a core–shell structure as a uniform model for simplicity. Our core–shell model is a completion of some previous models where a core–shell structure was considered, and essentially different from a popular model by which the problem was treated self-inconsistently leading to a magnetic size even smaller than the size of the core, as already discussed in [17]. Moreover, our core–shell structure is a magnetic one that may not be seen morphologically, which is different from cases where the core and shell are made of different materials [20,28].

3.2. Model fits

Using Eq. (6) to calculate numerically the magnetization curve of the uniform model for given values of T, we fix the values of the Boltzmann constant $k_B=1.38\times10^{-23}$ J/K and the permeability of free space $\mu_0=4\pi\times10^{-7}$ H/m, and change the values of parameters σ,D_0,χ, and $M_s(T)$ iteratively until the measured $\mu_0 M$ vs. $\mu_0 H$ curves for $T=300$ and 400 K are best fitted with a proper demagnetizing correction of $N_m=0.02$. Then, we fix the same data for σ,D_0, and χ and change $M_s(T)$ for $T=100$ and 200 K until the low and high field portions of the measured $\mu_0 M$ vs. $\mu_0 H$ curves are best fitted. All the four fitting curves are plotted as solid lines in Fig. 5(a), with fitting parameters listed.

For the core–shell model fits using Eq. (8), the values of $M_s(T)$ are set as four times those for the uniform model (as explained below), and the fitting curves are plotted in Fig. 5(b), with all fitting parameters listed. It should be noted that the data for $T=100$ and 200 K cannot be well fitted by using the same set of σ,D_0,δ, and χ as those used for higher temperatures. Since σ and D_0 should be T independent for the same assembly of particles and the effect of χ is small, this implies that at least δ should change with T and H if a core–shell model is still applied. Physically, this may be a consequence of the interaction occurring between the core and the shell, which will be discussed in Section 4.6.

It is necessary to make an explanation on the demagnetizing correction. In the measurements of our superparamagnetic powder, the magnetic moment and the applied field are measured accurately since the SQUID magnetometer has been properly calibrated and the field error owing to the magnetization of the superconducting wire has been corrected. However, there is still a demagnetizing effect to be considered. This effect can be neglected when the magnetic particles are very loosely packed, as in the case of [17], but it cannot in most cases. We propose a way to determine N_m in the present work by measuring $M(H)$ curves at more than two different T values and fitting them logically with the same set of parameters. It is shown that the fitting can be well done only when N_m is incorporated as an extra parameter, so that proper N_m is determined for the measured sample. Our experience shows that N_m cannot be larger than 0.02. Such a small N_m value comes from loosely packed particles in the sample; $N_m=0.02$ gives a rough estimate of the volume fraction of the nickel particles in the sample, which is about 0.1 in the present case.

It is important to mention that such a demagnetizing correction was not performed in most works on magnetic properties of assemblies of magnetic fine particles, so that low-field superparamagnetic susceptibility χ_0 obeying the Curie law was modified to one obeying the Curie–Weiss law. In our case, the Curie law may be expressed by $\mu_0^2 M_s^2/\chi_0\propto T$ [17], where the average values of $\mu_0 M_s$ in particles is given in Fig. 5(a) and χ_0 may be obtained from the experimental M/H at $\mu_0 H\approx0.004$ T. A comparison of $\mu_0^2 M_s^2/\chi_0$ vs. T before and after demagnetizing correction is shown in Fig. 6. We see that the Curie–Weiss relation $\mu_0^2 M_s^2/\chi_0\propto(T-T_c)$ with $T_c<0$ is changed into the Curie relation by the demagnetizing correction.

3.3. Size distribution

The log-normal probability density function $p(v;\mu,\sigma)$ of the particle volume distribution by volume, expressed by Eq. (4), may be converted into the probability density function of the particle diameter distribution by volume,

$$p(D)=\frac{3}{\sqrt{2\pi}\sigma D}\exp\left[-\frac{9(\ln D-\ln D_0)^2}{2\sigma^2}\right], \tag{10}$$

where particle diameter

$$D=(6v/\pi)^{1/3}. \tag{11}$$

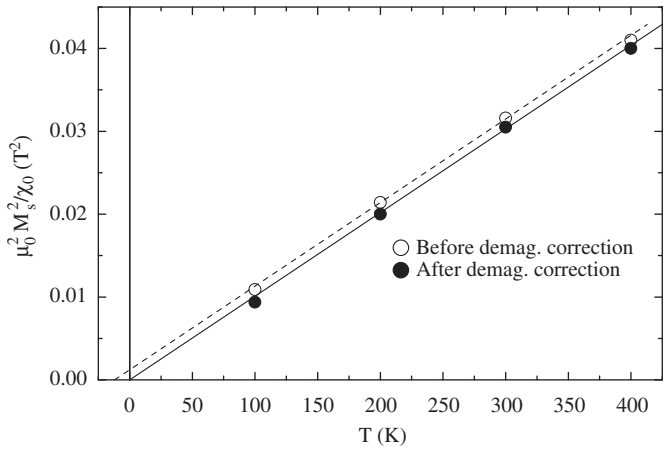

Fig. 6. Influence of demagnetizing correction on M_s^2/χ_0 vs. T relation. The solid and dashed lines show the linear relations of the Curie and the Curie–Weiss laws, respectively.

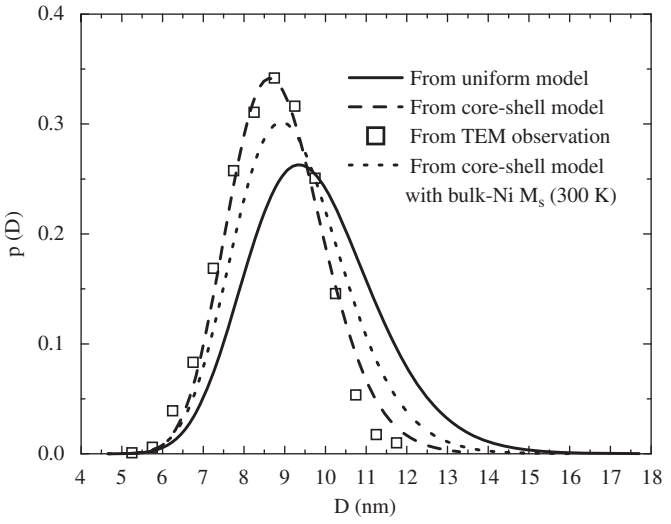

Fig. 7. Particle size distribution by volume obtained from magnetization curve fits by the uniform (solid line) and core–shell models (dashed line) and from TEM images (open squares). The dotted line is obtained from the core–shell model fit at $T=300$ K with $\mu_0 M_s = 0.607$ T, the value of bulk nickel.

The $p(D)$ vs D curves calculated from $D_0=9.6$ nm and $\sigma = 0.48$ for the uniform model fits and from $D_0=8.8$ nm and $\sigma = 0.4$ for the core–shell model fits are plotted in Fig. 7 by solid and dashed lines, respectively. We see that the former distribution is wider than the latter with its maximum located at larger D. The square symbols are the size distribution by volume evaluated by measuring more than 550 nanoparticles from the TEM image in Fig. 1; it shows a good coincidence with the dashed line. In fact, the fitting parameters of the core–shell model have been chosen iteratively by comparing the modeling distribution curve with the TEM results.

4. Discussion

4.1. Polycrystalline nanoparticles

Since the X-ray intensity is proportional to the total particle volume and the peak width is directly related to the particle size, the particle diameter determined directly from XRD patterns using the Scherrer relation is the particle-volume-weighted average diameter [17]

$$D_{vd} = \int_0^\infty p(v;\mu,\sigma) D(v)\, dv. \tag{12}$$

$D_{vd}=8.9$ nm is calculated using $D_0=8.8$ nm and $\sigma = 0.4$ for the core–shell model fits, which is consistent with TEM observation. This D_{vd} is roughly twice the average $D_{\mathrm{RXD}}=4.6$ nm for the crystallites, so that the nickel particles shown in the TEM images are polycrystalline in general. This is different from the case of ferrimagnetic iron-oxide particles, whose particles observed in TEM are single crystals [17,18].

Since D_{XRD} determined from the (2 0 0) peak is significantly smaller than that determined from the (1 1 1) peak, the crystallites seem to have a cube-like shape.

4.2. Superparamagnetism

As shown in Fig. 5, there is no hysteresis occurring in the magnetization loops for T between 100 and 400 K, i.e., the thermal energy is sufficient to equilibrate the magnetization at each field value in the time of experiment, so that the assembly of the studied nickel nanoparticles may be superparamagnetic in this T range. Being polycrystalline, each particle is a single magnetic domain, since after a proper demagnetizing correction, the measured magnetization curves at $T=300$ and 400 K can be well fitted by the uniform model of superparamagnetism with the same set of parameters. However, to further confirm the superparamagnetism, the magnetization curves at lower T should also be well fitted with the same set of D_0 and σ values, since the sizes of the particles should not be T dependent, and both D_0 and σ parameters should define a size distribution that is consistent with the one determined by TEM measurements. These two requirements may be fulfilled by using the core–shell model fits, as discussed below.

4.3. Model fits and particle sizes

The uniform model fits lead to over-large D_0 and σ, which results in a wider particle size distribution centered at a larger D compared with the TEM size distribution (Fig. 7). As shown in [17], the same magnetization curve may be equally well fitted by either the uniform model or the core–shell model, and the D_0 and σ obtained by the core–shell model fitting are smaller than those obtained by the uniform model fitting. Increasing the shell thickness δ and the M_s in the core to fit the magnetization curves by the core–shell model, we find a set of parameters listed in Fig. 5(b) that are best in agreement with the TEM data.

The advantage of the core–shell model over the uniform model is not shown by a better fitting quality to the $M(H)$ curves but by the obtained size distribution to be closer to the TEM data. In principle, an increase in M_s could be compensated by a decrease in v_c to maintain constant $M_s v_c$ in Eq. (9), so that a size distribution that is most close to the TEM one may be obtained by changing both freely. However, in order to maintain the same distribution of $M_s v_c$, the increase in M_s and decrease in v_c have to be realized by increasing δ and decreasing D_0 and σ simultaneously. The reason for D_0 and σ determined from the core–shell model fits to be smaller than those from the uniform model can be understood as follows. In the core–shell model, the contribution of the shell of a certain thickness to superparamagnetism is removed, and the shell occupies a larger volume fraction in smaller particles than in larger particles. As a result, the total particle size distribution with smaller D_0 and σ obtained by the core–shell model fits will give

practically the same $M_s v_c$ distribution as that obtained by uniform model fits with larger D_0 and σ.

4.4. Magnetic structure

The goodness of the core–shell model fits indicates the existence of a core–shell magnetic structure in the nickel nanoparticles.

Different from the case of ferrimagnetic iron oxide, for which the M_s in the core is the same as that for the bulk, the M_s in the core of nickel nanoparticles can be greater than its bulk value. The $\mu_0 M_s(T)$ data points resulting from the uniform and core–shell model fits are drawn in Fig. 8, where, for comparison, a solid curve is plotted for bulk nickel, calculated from

$$M_s(T) = M_s(0)[1-0.15(T/T_c)^{3/2}-0.85(T/T_c)^{5/2}]^{1/3}, \quad (13)$$

where $M_s(0)=0.65$ T and $T_c=630$ K [33], and the dashed and dotted curves are drawn artificially for the uniform and core–shell model results to have the same T_c as the bulk. We see that although the M_s for the uniform model is always much smaller than that for the bulk, the M_s in the core could be significantly larger.

This difference in magnetic structure between ferromagnetic and ferrimagnetic nanoparticles suggests the difference in the nature of magnetic ordering. As described in [34], the magnetic ordering in ferrimagnetic iron oxides results from the local superexchange interaction between the 3d electrons of iron ions with certain magnetic moments through the oxygen ions in between, and when the surface effects reduce the interaction so that M_s becomes zero in a surface layer, M_s in the core remains its bulk value. The detailed mechanisms for the zero M_s in the surface layer were studied in [10–13].

For ferromagnets, however, $M_s(0)$ comes from the 3d electrons itinerant among the atoms, so that the discrete energy levels for isolated atoms are extended to certain spin-up and spin-down energy bands splitted by exchange field. Since both bands are partially overlapped in energy, so that the spontaneous magnetic moment per ion, given by the difference in the number of electrons in the spin-up and the spin-down bands, is about $0.6\mu_B$, which is much smaller than $2\mu_B$ ($\mu_0 M_s \approx 2.1$ T), expected by 2 vacancies in the 3d shell of nickel atom [34]. For a nano-sized particle, the spin-up and spin-down bands should be energetically narrower than those for the bulk with less overlap in the same exchange field, so that $\mu_0 M_s(0)$ being between 0.65 and 2.1 T may be expected. The core–shell model fits indicate that such an enhancement in M_s occurs only in the core, and they should require that the exchange effects be weakened (or even change the sign to antiferromagnetic coupling) near the particle surface, leading to a very small M_s in the shell. As to the paramagnetism, it should be Pauli paramagnetism resulting from the band structure, so that χ is approximately temperature independent [34].

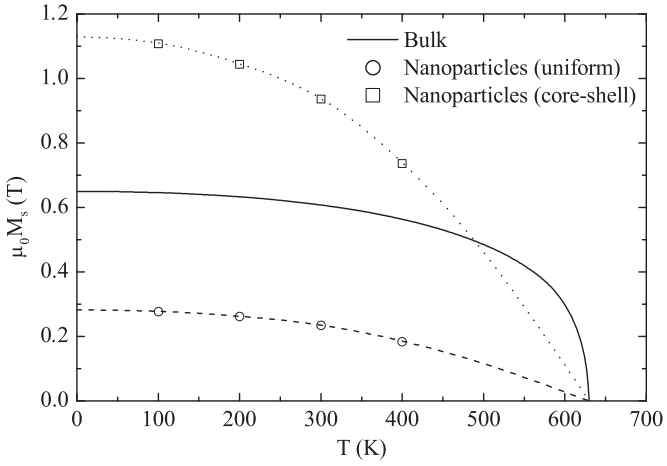

Fig. 8. Spontaneous magnetization M_s as a function of temperature T. Symbols are for the nickel nanoparticles obtained from model fits in Fig. 4(a) and (b) and solid line is for the bulk nickel calculated from Eq. (13).

4.5. Comparison with previous works

The temperature dependence of M_s shown in Fig. 8 deduced from the core–shell model fits is qualitatively similar to that found in [26], where magnetization of nickel nanoparticles of average diameter 3 nm was detected by Kerr ellipticity at $T > 300$ K, and explained by quantum Monte-Carlo simulations considering Ising spins in a nanocube [22]. However, fitting the experimental $M(H,T)$ by a uniform model without considering a size distribution, the authors of [26] obtained a spontaneous magnetic moment per ion to be $2.5\mu_B$ per atom, which is a value 10 times larger than our result without physical basis.

M_s of nickel particles was found to decrease quickly with decreasing particle size in [19], which is consistent with our results. By Langevin function fitting with a uniform model in [24], M_s of nickel nanoparticles of TEM size about 3.3 nm was found approximately the same as that of bulk nickel with "magnetic" size about 5 nm. This seems to be consistent with our results, since the disagreement between the two sizes could be resolved by a core–shell model fit to get M_s in the core much larger than M_s of bulk nickel. M_s of nickel nanoparticles in silica gel was found to be about 90% of M_s of bulk nickel for particle sizes between 3 and 10 nm in [20]. This would help to understand the magnetic structure in nickel particles by showing significant influence of silica gel if it is further confirmed.

In a study of nickel nanoparticles [28], a synthesis procedure similar to ours was adopted with polycrystalline fcc grains obtained. Since the high-field magnetization was found to be, similarly to our case, significantly smaller than that for bulk nickel, the existence of an amorphous antiferromagnetic NiO shell was assumed. The shell thickness was estimated to be around 1 nm by assuming the bulk-nickel M_s value in the core and using the densities for bulk nickel and bulk NiO in the core and the shell, respectively. Different from that approach, we have assumed the particles are pure nickel and determined the shell thickness by careful uniform and core–shell model fits to the entire magnetization curves with the same set of D_0 and σ parameters at different temperatures, and comparing the resulting size distribution with TEM measurements, so that the thicker shell is found with the M_s in the core to be greater than that for the bulk nickel. We should emphasize that using the bulk-nickel M_s for the core, not only the core–shell model fit gives overlarge D_0 and σ, but the resultant D_0 and σ are also unphysically T dependent. As an example, we show the size distribution curve (dotted line) obtained by the core–shell model fit at $T=300$ K with $\mu_0 M_s = 0.607$ T in Fig. 7.

4.6. Possible exchange interaction between the core and the shell

The M_s in the core resultant from the core–shell model fits is significantly larger than what was measured and calculated for small nickel clusters in [35–37]. The magnetism from the atom to the bulk in nickel clusters was studied by measuring the clusters deflections of a molecular beam in an inhomogeneous magnetic field in [35] and the measurements were improved in [36]. According to [36], the spontaneous moment per atom decreases from 1.8 to $0.68\mu_B$ with increasing the atom number per cluster from 5 to 740, showing a tendency of further decrease at even

larger atom numbers. The variation up to a cluster of 60 atoms was explained by calculating the spin-polarized electronic structure with a self-consistent tight-binding method considering 3d, 4s, and 4p valence electrons [37]. The core of our nickel particles of diameter $D_0-2\delta=5.6$ nm contains about 10^4 atoms, which is one order of magnitude more than the upper limit studied in [35,36], and corresponds to a moment of $1.04\mu_B$ per atom. This over-large M_s in the core might be related to the difference in atomic structure; the clusters have quite different structures from fcc as in our case. But more reasonably, the resultant over-large M_s in the core may be a consequence of interaction between the core and the shell, which is not considered in our core–shell model.

The large M_s variation in ferromagnetic nanoparticles is a new phenomenon that has to be properly explained. Its explanation turns out to be difficult, since unlike the case of ferrites whose magnetic ordering occurs among 3d electrons localized in each iron ion, the band theory explaining magnetic ordering of ferromagnets itself is defined for the whole body with ignored local variation of magnetization. The spherical particles consisting of few cubic crystallites suggest the existence of a spherical amorphous shell containing oxygen atoms with an antiferromagnetic properties. If this is true, the discovered magnetic core–shell structure would be directly linked to a core–shell microstructure, and the magnetization rotations in the core would not only be driven by the applied field but also be impeded by an opposite exchange field owing to the exchange interaction between the ferromagnetic core and the antiferromagnetic shell. As a result, the low-field susceptibility of the assembly should be reduced from what is calculated from the Langevin function without considering the core–shell interaction. If the exchange field is relatively larger for smaller particles than for larger particles, then smaller particles contribute to the reduction of susceptibility more than larger particles. In this case, the large increase in δ and M_s required to explain the anomalous size distribution may be partially replaced by the effect of the exchange field. In other words, the required M_s in the core can be smaller if the exchange interaction between the core and the shell is considered. If such an interaction is T and H dependent, then the anomalies occurring in the low-T M vs. H curves, formally explained by a T and H dependent δ, may be understood on a more fundamental level.

5. Conclusion

A core–shell model developed for the study of ferrimagnetic oxide nanoparticles is used for metallic ferromagnets. Values of M_s in the core larger than its bulk value may result from the model fits to obtain a correct particle size distribution, which is different from the case of ferrimagnets, whose M_s is the same for the core and the bulk. Such a difference in model fits reflects the difference in magnetic ordering mechanism. The magnetic ordering in oxide ferrites is due to the superexchange interaction between neighboring spins of iron ions, with fixed moments, through oxygen ions, whereas for metallic ferromagnets, it comes from the slip of spin-up and spin-down bands of the entire body by direct exchange interaction. The bands for nanoparticles are energetically narrower than those for the bulk, so that $M_s(0)$ for the former is larger than for the latter. However, the mechanism of magnetic core–shell structure in ferromagnetic nanoparticles is unclear, and the resultant M_s in the core is over large compared with previous calculations on nickel clusters. Nevertheless, if the core and the shell may be regarded as ferromagnetic and antiferromagnetic, respectively, then the difficulty of over-large M_s in the core may be overcome by considering the exchange interaction between the core and the shell.

Acknowledgments

We are grateful to D. Givord for his valuable comments. Partial financial support from the Ministerio de Cíencia e Innovacion (MAT2009-08024 and CONSOLIDER-NANOSELECT-CSD2007-00041), the Generalitat de Catalunya (2009SGR203 and FI Grant of OP), and the CSIC (CRIMAFOT-PIF08-016) is acknowledged.

References

[1] Q.A. Pankhurst, J. Connolly, S.K. Jones, J. Dobson, J. Phys. D Appl. Phys. 36 (2003) R167.
[2] G. Bate, in: E.P. Wohlfarth (Ed.), Ferromagnetic Materials, vol. 2, North-Holland, Amsterdam1980, p. 381.
[3] S.W. Charles, J. Popplewell, in: E.P. Wohlfarth (Ed.), Ferromagnetic Materials, vol. 2, North-Holland, Amsterdam1980, p. 509.
[4] C.P. Bean, J. Appl. Phys. 26 (1955) 1381.
[5] C.P. Bean, I.S. Jacobs, J. Appl. Phys. 27 (1956) 1448.
[6] C.P. Bean, J.D. Livingston, J. Appl. Phys. 30 (1959) 120S.
[7] A.E. Berkowitz, W.J. Schule, P.J. Flanders, J. Appl. Phys. 39 (1968) 1261.
[8] R. Kaiser, G. Miskolczy, J. Appl. Phys. 41 (1970) 1064.
[9] R.E. Rosensweig, Ferrohydrodynamics, Cambridge University Press, Cambridge, 1985, p. 60.
[10] J.M.D. Coey, Phys. Rev. Lett. 27 (1971) 1140.
[11] R.H. Kodama, A.E. Berkowitz, E.J. McNiff Jr., S. Foner, Phys. Rev. Lett. 77 (1996) 394.
[12] B. Martinez, X. Obradors, Ll. Balcells, A. Rouanet, C. Monty, Phys. Rev. Lett. 80 (1998) 181.
[13] H. Kachkachi, M. Dimian, Phys. Rev. B 66 (2002) 174419.
[14] A. Millan, A. Urtizberea, N.J.O. Silva, F. Palacio, V.S. Amaral, E. Snoeck, V. Serin, J. Magn. Magn. Mater. 312 (2007) L5.
[15] R.C. Woodward, J. Heeris, T.G.St. Pierre, M. Saunders, E.P. Gilbert, M. Rutnakornpituk, Q. Zhang, J.S. Riffle, J. Appl. Cryst. 40 (2007) s495.
[16] P.P. Vaishnava, U. Senaratne, E.C. Buc, R. Naik, V.M. Naik, G.M. Tsoi, L.E. Wenger, Phys. Rev. B 76 (2007) 024413.
[17] D.-X. Chen, A. Sanchez, E. Taboada, A. Roig, N. Sun, H.-C. Gu, J. Appl. Phys. 105 (2009) 083924.
[18] D.-X. Chen, N. Sun, H.-C. Gu, J. Appl. Phys. 106 (2009) 063906.
[19] W. Gong, H. Li, Z. Zhao, J. Chen, J. Appl. Phys. 69 (1991) 5119.
[20] C. Estournes, T. Lutz, J. Happich, T. Quaranta, P. Wissler, J.L. Guille, J. Magn. Magn. Mater. 173 (1997) 83.
[21] X. Sun, A. Gutierrez, M.J. Yacaman, X. Dong, S. Jin, Mater. Sci. Eng. A286 (2000) 157.
[22] D. Gerion, A. Hirt, I.M.L. Billas, A. Chatelain, W.A. de Heer, Phys. Rev. B 62 (2000) 7491.
[23] P. Zhang, F. Zuo, F.K. Urban III, A. Khabari, P. Griffiths, A. Hosseini-Tehrani, J. Magn. Magn. Mater. 225 (2001) 337.
[24] F.C. Fonseca, G.F. Goya, R.F. Jardim, R. Muccillo, N.L.V. Carreo, E. Longo, E.R. Leite, Phys. Rev. B 66 (2002) 104406.
[25] H. Amekura, H. Kitazawa, N. Kishimoto, Nucl. Instr. Methods Phys. Res. B 219–220 (2004) 825.
[26] H. Amekura, Y. Fudamoto, Y. Takeda, N. Kishimoto, Phys. Rev. B 71 (2005) 172404.
[27] Y. Chen, D.L. Peng, D. Lin, X. Luo, Nanotechnology 18 (2007) 505703.
[28] A.C. Johnston-Peck, J. Wang, J. Tracy, ACSNANO 3 (2009) 1077.
[29] F. Davar, Z. Fereshteh, M. Salavati-Niasari, J. Alloys Compd. 476 (2009) 797.
[30] J.I. Langford, D. Louër, P. Scard, J. Appl. Cryst. 33 (2000) 964.
[31] D.-X. Chen, R.B. Goldfarb, J. Appl. Phys. 66 (1989) 2489.
[32] D.-X. Chen, J.A. Brug, R.B. Goldfarb, IEEE Trans. Magn. 27 (1991) 3601.
[33] M.D. Kuz'min, Phys. Rev. Lett. 94 (2005) 107204.
[34] S. Chikazumi, Physics of Ferromagnetism, Oxford University Press, 1997.
[35] I.M.L. Billas, A. Chatelain, W.A. de Heer, Science 265 (1994) 1682.
[36] S.E. Apsel, J.W. Emmert, J. Deng, L.A. Bloomfield, Phys. Rev. Lett. 76 (1996) 1441.
[37] F. Aguilera-Granja, S. Bouarab, M.J. Lopez, A. Vega, J.M. Montejano-Carrizales, M.P. Iniguez, J.A. Alonso, Phys. Rev. B 57 (1998) 12469.